Chemical Geology 455 (2017) 120–130

Contents lists available at ScienceDirect

Chemical Geology

journal homepage: www.elsevier.com/locate/chemgeo

Mantle melting versus mantle metasomatism – "The chicken or the egg" dilemma

Ekaterina S. Kiseeva [a,*], Vadim S. Kamenetsky [b], Gregory M. Yaxley [c], Simon R. Shee [d]

[a] Department of Earth Sciences, University of Oxford, Oxford, OX1 3AN, UK
[b] ARC Centre of Excellence in Ore Deposits and School of Earth Sciences, University of Tasmania, Hobart, TAS 7001, Australia
[c] Research School of Earth Sciences, The Australian National University, Canberra, ACT, 2601, Australia
[d] Unit 3, 13 Hyland Street Foster, Victoria 3960, Australia

ARTICLE INFO

Article history:
Received 22 May 2016
Received in revised form 13 October 2016
Accepted 18 October 2016
Available online 19 October 2016

Keywords:
Kimberlite-borne xenolith
Roberts Victor
Carbonated eclogite
Incipient melting
Cratonic mantle
Secondary mineral assemblage

ABSTRACT

Most eclogitic mantle xenoliths brought to the surface exhibit a certain degree of enrichment with incompatible elements, usually attributed to the effect of mantle metasomatism by a putative metasomatic fluid. The metasomatic overprint is represented mainly by enrichments in Na, K, Ba, Ti and LREE and the original source of this fluid remains unknown. In this paper, we present a detailed petrological study of a typical eclogitic mantle xenolith from the Roberts Victor kimberlite mine in South Africa. We find that its textural and mineralogical features present strong evidence for incipient melting. The melting assemblage we observe did not necessarily require introduction of additional components, that is: in-situ melting alone could produce highly incompatible element enriched melt without involvement of a hypothetical and speculative "metasomatic event". Due to the higher abundance in incompatible elements and lower solidus temperature than peridotites, mantle eclogites, some of which represent previously subducted oceanic crust, are much more plausible sources of mantle metasomatism, but on the other hand, they can be considered as highly metasomatised themselves. This brings us to the "chicken or egg" dilemma – was the secondary mineral assemblage in mantle lithologies a result or a source of mantle metasomatism?

1. Introduction

Studies of metasomatism date back to Goldschmidt (1922), who defined it as "*a process of alteration which involves enrichment of the rock by new substances brought in from the outside*". The importance of mantle metasomatism has been widely acknowledged since there are hardly any investigations of either mantle xenoliths or conclusions about the inferred sources of intraplate magmas in both continental and oceanic settings that do not invoke metasomatic changes to some degree. Introduction of "metasomatic" components affects the chemistry of the original mantle rock and decreases its solidus temperature, meaning that mantle metasomatism or enrichment in highly incompatible elements should be considered one of the main driving forces of mantle melting.

The origin of putative metasomatic fluids is mysterious, with two potential sources being either subducted slabs, or mantle plumes. The two main types of metasomatic alteration, observed in most lithospheric mantle xenoliths, are "modal" (petrographically visible due to replacement textures and development of secondary, usually hydrous phases) and "cryptic" (with enrichment in trace and rare earth elements (REE), but without petrographic evidence of metasomatism, i.e. no secondary minerals are formed) (Dawson, 1984). These metasomatic overprints are usually so complex that they are considered to have been caused by multiple metasomatic events (e.g. Heaman et al., 2006; Huang et al., 2014; Misra et al., 2004).

Interestingly, although all recovered mantle xenoliths are interpreted to have been metasomatised by an external agent, there are few reports in the literature on the source of the agent itself, i.e. which lithology partially melted, dehydrated or decarbonated to produce a melt or a fluid capable of metasomatising the surrounding mantle? This represents a classic "chicken or the egg" dilemma: how do we recognise a mantle rock, which was a source of metasomatising melt/fluid, and why was this particular rock not a subject of prior alteration?

To address these questions, we undertook a detailed petrological study of primary and secondary phases of an eclogite xenolith from the Roberts Victor kimberlite pipe (South Africa). We evaluate the possible role of incipient eclogite melting in producing in-situ secondary mineral assemblages. Additionally, we suggest that altered oceanic

* Corresponding author.
E-mail address: Kate.Kiseeva@earth.ox.ac.uk (E.S. Kiseeva).

http://dx.doi.org/10.1016/j.chemgeo.2016.10.026

crust has sufficient alkali- and volatile components to account for mineralogical and geochemical features of incipient melting in eclogites without addition of any metasomatic fluid or melt.

2. Sample selection and methods

2.1. SS2 eclogite xenolith

SS2 is a diamond-free eclogite xenolith, about 20 × 15 × 7 cm in size, from the Roberts Victor kimberlite pipe (South Africa) (Fig. 1). The xenolith is a typical example of eclogite xenoliths from this pipe. It is bimineralic, with roughly equal proportions of coarse-grained omphacitic clinopyroxene and pyrope-almandine garnet (Table 1, Fig. 1a), which are interpreted as primary phases. The P-T (pressure-temperature) conditions of garnet and clinopyroxene equilibration are estimated to be between 1165 and 1205 °C (Ellis and Green, 1979) and between 1105 and 1150 °C (Krogh, 1988) for pressures between 5 and 6 GPa. This is in a good agreement with the P-T values for Roberts Victor eclogites reported by Huang et al. (2012).

The classification of eclogite xenoliths from Roberts Victor into two distinctive groups was initially proposed by MacGregor and Carter (1970) and followed by subsequent studies (e.g. Gréau et al., 2011; Huang et al., 2012; McCandless and Gurney, 1989; Schulze et al., 2000). According to McGregor and Carter's classification, Type I eclogites contain coarse-grained subhedral to rounded garnet that is surrounded by anhedral clinopyroxene. Unlike in the Type II eclogites, the Type I garnet and clinopyroxene do not show an interlocking texture and contain large amounts of a secondary mineral assemblage that surrounds every grain. Clinopyroxene from Type I is more altered than in Type II with each grain being surrounded and cross cut by zones of secondary or spongy clinopyroxene. Type I eclogites also contain abundant inclusions of phlogopite, sulfide and rutile, observed in the SS2 xenolith. Huang et al. (2012) also pointed out that Type I eclogites are more metasomatically altered than Type II and are richer in LREE (light REE) and LILE (large-ion lithophile elements). The chemical classification proposed by McCandless and Gurney (1989) aimed to distinguish between the Type I and Type II eclogites using the alkali contents of garnet and clinopyroxene (Fig. 2a). Type I eclogites could be defined by ≥0.09 wt% Na_2O in garnet or ≥0.07 wt% K_2O in clinopyroxene. We also find that the concentration of TiO_2 in both garnet and clinopyroxene could potentially be a valid discriminator (Fig. 2b). Thus, based on its textural and compositional characteristics, the SS2 xenolith, described in this study, can be classified as a Type I eclogite (Gréau et al., 2013; McCandless and Gurney, 1989; MacGregor and Carter, 1970).

2.2. Analytical methods

Thin sections and an epoxy mount were prepared from SS2 eclogite. Back-scattered electron images were obtained using a Hitachi SU-70 Schottky field emission SEM at University of Tasmania (UTAS) and a Hitachi 4300 field emission SEM at the Centre for Advanced Microscopy, Australian National University (ANU). These were used to characterise textural relationships.

Quantitative major element analyses of minerals were obtained using a Cameca SX100 Electron probe Microanalyser (EPMA) at the Central Science Laboratory, University of Tasmania (UTAS). The operational conditions were 15 kV accelerating voltage, 10 nA beam current and a 10 μm spot with natural plagioclase, hornblende, olivine and clinopyroxene chosen as primary and secondary standards. Secondary mineral assemblages in veins and melt pockets were analysed with 15 μm defocused beam. Table 1 presents averages of 7–10 spot analyses

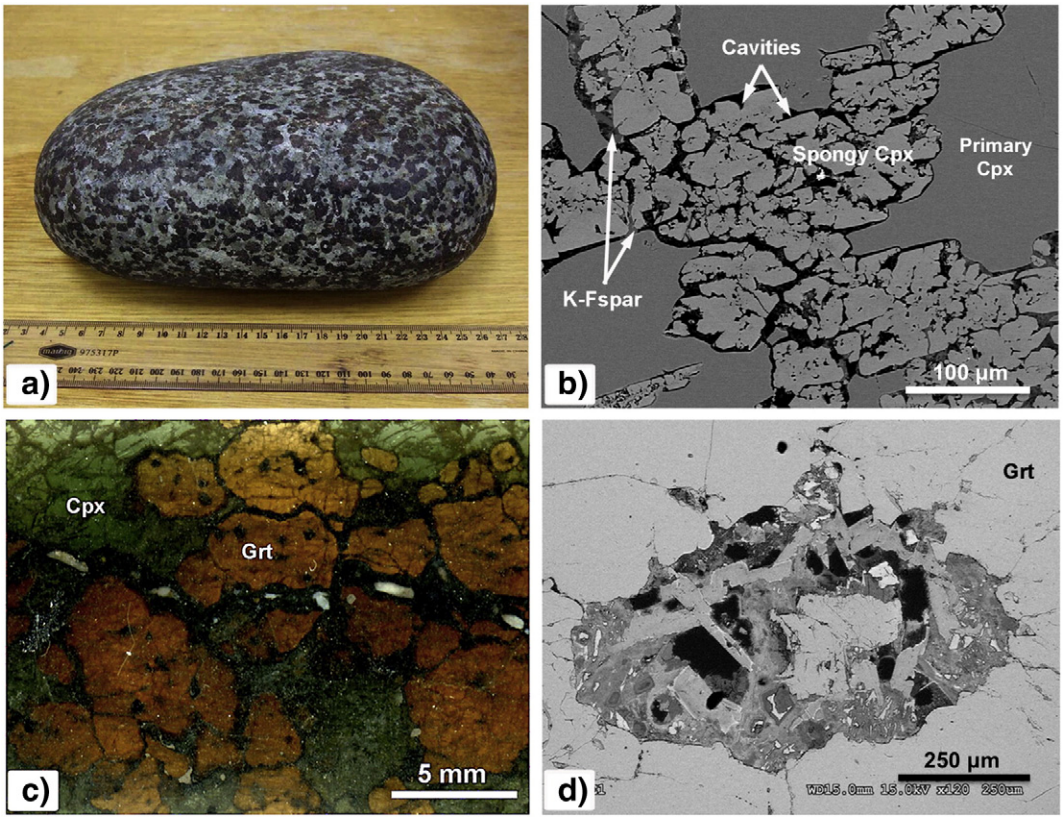

Fig. 1. (a) The original SS2 eclogite xenolith from Roberts Victor mine, South Africa. (b) Back-scattered image of spongy-textured Na-poor clinopyroxene embedded into the Na-rich primary clinopyroxene. Some of the cavities are filled with Na-rich and K-rich silicates. (c) Scanned part of the thin section that was studied in this work. A large vein is cross-cutting the sample, small rims filled with melting products surround every garnet and clinopyroxene crystal. White phases in veins are melt pools. See text for more explanation. (d) Back-scattered image of melt pocket in garnet, includes calcite, phlogopite, spinel, amphibole and Na-Si-rich phases. Cpx - clinopyroxene, K-Fspar - K-feldspar.

Table 1
Major element compositions of the primary phases and melting assemblage.

	Cpx primary	σ	Cpx spongy	σ	Garnet	σ	Phlogopite	σ	Amphibole	σ	Plagioclase	σ	Zeolite 1	σ	Zeolite 2	σ	Calcite	σ	K-Feldspar	σ	Bulk secondary*	σ
SiO_2	54.59	0.38	52.48	0.93	39.90	0.24	36.93	0.77	39.87	1.85	57.03	1.42	45.91	1.44	52.14	0.47	b.d.l.	–	61.13	1.53	44.04	7.29
TiO_2	0.38	0.03	0.47	0.11	0.30	0.03	4.18	0.55	2.19	1.51	0.10	0.03	b.d.l.	–	b.d.l.	–	b.d.l.	–	0.17	0.18	0.19	0.20
Al_2O_3	6.77	0.17	4.22	1.30	22.91	0.28	15.90	1.10	16.04	1.70	26.47	0.99	27.77	0.72	24.60	0.53	b.d.l.	–	19.06	0.49	17.30	5.91
Cr_2O_3	0.17	0.06	0.17	0.05	0.17	0.04	0.18	0.06	0.21	0.08	b.d.l.	–	b.d.l.	–	b.d.l.	–	b.d.l.	–	b.d.l.	–	0.09	0.06
V_2O_3	b.d.l.	–	b.d.l.	–	b.d.l.	–	0.12	0.12	0.09	0.11	b.d.l.	–	b.d.l.	–	b.d.l.	–	b.d.l.	–	b.d.l.	–	n.m.	–
MgO	12.08	0.15	14.62	1.26	14.68	0.10	16.20	0.22	14.26	2.90	b.d.l.	–	b.d.l.	–	b.d.l.	–	b.d.l.	–	0.55	0.49	11.85	6.03
CaO	14.29	0.26	17.56	1.60	4.22	0.14	b.d.l.	–	8.14	2.89	7.60	1.08	0.91	0.91	0.40	0.40	57.08	0.43	0.54	0.50	1.88	2.02
MnO	0.12	0.03	0.15	0.04	0.52	0.02	0.11	0.04	0.33	0.10	b.d.l.	–	b.d.l.	–	b.d.l.	–	0.70	0.02	b.d.l.	–	0.29	0.12
FeO	6.23	0.22	7.47	0.59	17.17	0.19	11.14	0.25	12.84	2.54	0.80	0.38	0.20	0.13	0.19	0.32	0.22	0.18	1.37	0.95	12.13	5.05
BaO	b.d.l.	–	b.d.l.	–	b.d.l.	–	0.44	0.10	b.d.l.	–	0.22	0.04	b.d.l.	–	0.10	0.14	b.d.l.	–	0.77	0.45	n.m.	–
SrO	b.d.l.	–	b.d.l.	–	b.d.l.	–	b.d.l.	–	b.d.l.	–	0.17	0.07	0.42	0.54	b.d.l.	–	0.13	0.11	0.11	0.21	n.m.	–
Na_2O	4.22	0.12	1.87	1.15	0.08	0.02	0.53	0.22	2.47	0.99	6.40	0.62	13.81	1.12	12.05	1.07	b.d.l.	–	1.14	0.91	4.01	3.23
K_2O	0.14	0.01	b.d.l.	–	b.d.l.	–	9.38	0.28	0.67	0.27	0.65	0.16	b.d.l.	–	0.73	1.75	b.d.l.	–	14.42	1.57	0.35	0.31
P_2O_5	b.d.l.	–	b.d.l.	–	b.d.l.	–	b.d.l.	–	b.d.l.	–	b.d.l.	–	b.d.l.	–	b.d.l.	–	b.d.l.	–	0.12	0.13	0.07	0.05
CO_2	–	–	–	–	–	–	–	–	–	–	–	–	–	–	–	–	43.30	0.01	–	–	–	–
H_2O	–	–	–	–	–	–	4.08	0.01	2.04	0.01	–	–	–	–	–	–	–	–	–	–	–	–
Total	98.99		99.02		99.95		99.19		99.15		99.44		89.01		90.21		101.42		99.38		92.21	3.27

b.d.l. below detection limit; n.m. not measured; H_2O in phlogopite and amphibole and CO_2 in calcite were calculated according to stoichiometry.
* 179 spot analyses of the secondary mineral assemblages in veins and melt pockets analysed with 15 μm defocused beam. Note, they do not include "spongy" clinopyroxene textures and associated alkali-rich assemblage.

per phase. 179 spot analyses of the secondary assemblages were performed in order to obtain an average SiO_2 content (44 wt% SiO_2) later used as an internal standard for the Laser Ablation Inductively Coupled Plasma Mass Spectrometry (LA-ICPMS) analysis.

The sample was mounted in epoxy resin for LA-ICPMS analysis of trace elements. We used a Perkin Elmer Nexion quadrupole mass spectrometer coupled to a New Wave Research UP213 Nd:YAG laser at the University of Oxford. A beam diameter of 50 μm was employed for garnet, clinopyroxene and spongy clinopyroxene. Clinopyroxene analyses were repeated with a 100 μm beam diameter during a different LA-ICPMS session and the results of two sessions agreed within the uncertainty. Secondary mineral assemblages located on the grain boundaries and in small veins cross-cutting the xenolith were analysed using a 100 μm beam diameter.

The following masses were counted: ^{47}Ti, ^{85}Rb, ^{88}Sr, ^{89}Y, ^{90}Zr, ^{93}Nb, ^{138}Ba, ^{139}La, ^{140}Ce, ^{142}Nd, ^{152}Sm, ^{153}Eu, ^{158}Gd, ^{159}Tb, ^{164}Dy, ^{165}Ho, ^{166}Er, ^{174}Yb, ^{175}Lu, ^{180}Hf, ^{181}Ta, ^{232}Th, ^{238}U, with yields calibrated on NIST 610 glass standard as the primary standard. BCR-2G and NIST 612 glasses were chosen as secondary standards. No >8–9 unknowns were run between each set of standards. The internal reference element for all analysed phases was Si, previously measured by EPMA. The data for garnet were filtered to exclude contributions from multiple garnet-hosted melt inclusions. 44 wt% SiO_2 was chosen as the abundance of the internal reference element for the secondary assemblage with ~17% uncertainty (1σ) due to the high heterogeneity of the material represented by quenched phases. To minimise the uncertainty, 37 replicate analyses of the secondary assemblage were performed. Background was counted for the first 20 s, followed by a 40 s period of ablation. The background was minimised by a 60-second wash-out period between each analysis. The GLITTER (www.es.mq.edu.au/gemoc/glitter) software package was employed for the data reduction.

3. Results

3.1. Textural observations

Grains of primary garnet and clinopyroxene in SS2 are rarely in direct contact, but are rimmed by a fine-grained secondary assemblage (Fig. 1c). The main minerals within the secondary assemblage are amphibole, phlogopite, calcite, spinel, secondary clinopyroxene, zeolites and minor phases, such as rutile, apatite, sulfides and barite (Figs. 1, 3, 4, 5). Additionally, veins filled with the same secondary assemblage (Figs. 3b, 4d) cut across primary mineral grains. Zeolites (analcime and natrolite) compose rounded and irregularly shaped pools that were likely to have been formerly occupied by melt (Figs. 3a-d, 4a-c,f). Euhedral calcite crystals have grown from the walls inside these pools (Fig. 3a,c,d).

Apart from the intergranular phase assemblage, both primary garnet and clinopyroxene contain secondary minerals included in the coarse, primary crystals. In garnet, these are usually rounded pockets (up to 300 μm) containing an assemblage similar to that observed in the cross-cutting veins and along the grain boundaries (Fig. 1d).

Primary clinopyroxene contains bands and patches of secondary "spongy" clinopyroxene and alkali-rich phases (Figs.1b, 5a). The "spongy" clinopyroxene is the dominant secondary mineral assemblage formed around and within the primary clinopyroxene. The "spongy" clinopyroxene is surrounded by large cavities, Na- and K-rich glass-like material and/or a small amount of K-feldspar. Because of the small size, it is impossible to determine whether the glass is fully recrystallised into the feldspar or some of it is still preserved. Sometimes, a Ba-, Sr- and S-rich phase occurs in small veins together with the K-feldspar. Unlike the secondary assemblage present in cross cutting veins and melt pockets within the primary phases, the "spongy" clinopyroxene assemblage does not contain zeolites.

Carbonate-rich and two sulfur-rich assemblages (sulfate, present as small, 10–20 μm wide veins of barite, and Fe-rich sulfide with minor Ni

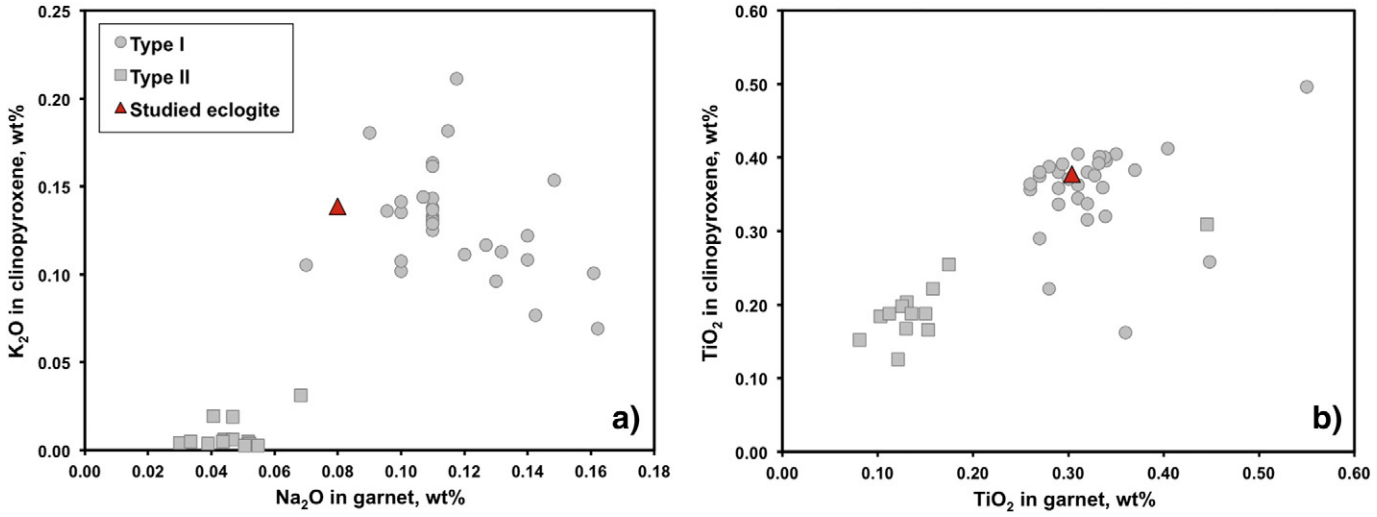

Fig. 2. Major element compositions of garnet and clinopyroxene from SS2. (a) Na_2O in garnet plotted against K_2O in clinopyroxene, previously used by McCandless and Gurney (1989) to discern between the Type I and Type II eclogites. (b) TiO_2 in garnet and clinopyroxene, which shows a similar pattern to panel (a). Grey symbols are garnets and clinopyroxenes from Huang et al. (2012, 2014).

and Cu) are observed along with the secondary silicate phases in veins and inclusions and along grain boundaries between primary garnet and clinopyroxene (Figs. 3b, 4a,c,e). The sulfide assemblage forms pools of different size (from few microns to a thousand microns) and of uneven shape. These pools are usually severely altered, with hematite and chlorite veinlets cutting through (Fig. 4e). Additionally, some of the barite can be found in the form of euhedral crystals. Anhedral barite is located within the veins of the secondary mineral assemblage as well as substituting and rimming Fe-sulfide and rutile (Figs. 3b, 4c). Rutile contains exsolution lamellae of ilmenite (Figs. 4b, 5b).

3.2. Major element compositions of primary and secondary phases

Major element compositions for all analysed phases are presented in Table 1. Garnet compositions are similar to the one reported for Type I eclogites by Huang et al. (2012). It is predominantly pyrope-almandine and contains 17.2 wt% FeO, 22.9 wt% Al_2O_3, 14.7 wt% MgO and 4.22 wt% CaO. Primary clinopyroxene is omphacitic in composition and contains 4.22 wt% Na_2O, 6.77 wt% Al_2O_3, 6.23 wt% FeO, 12.08 wt% MgO and 14. 3wt% CaO. The "spongy" clinopyroxene is diopsidic, with 1.87 wt% Na_2O, 17.6 wt.% CaO and 4.22 wt.% Al_2O_3 in comparison to the primary

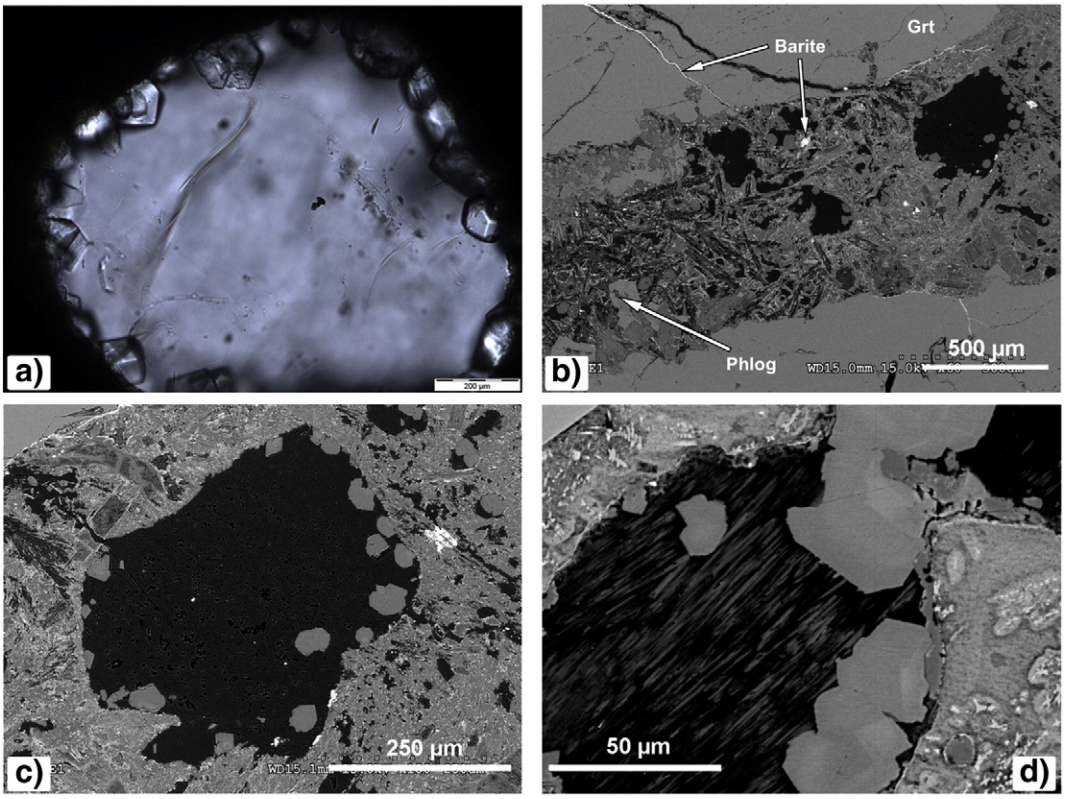

Fig. 3. (a) Optical image of euhedral calcite crystals growing into the melt pool, currently filled with zeolite aggregates. (b) Veinlet with melting products on a boundary between two primary garnet crystals. (c) A blown-up area of panel (b) with calcite crystals growing into the melt pool. (d) Zoned calcite crystals with darker parts more enriched in Sr (up to 1.1 wt% SrO). All panels, except (a) are back-scattered images.

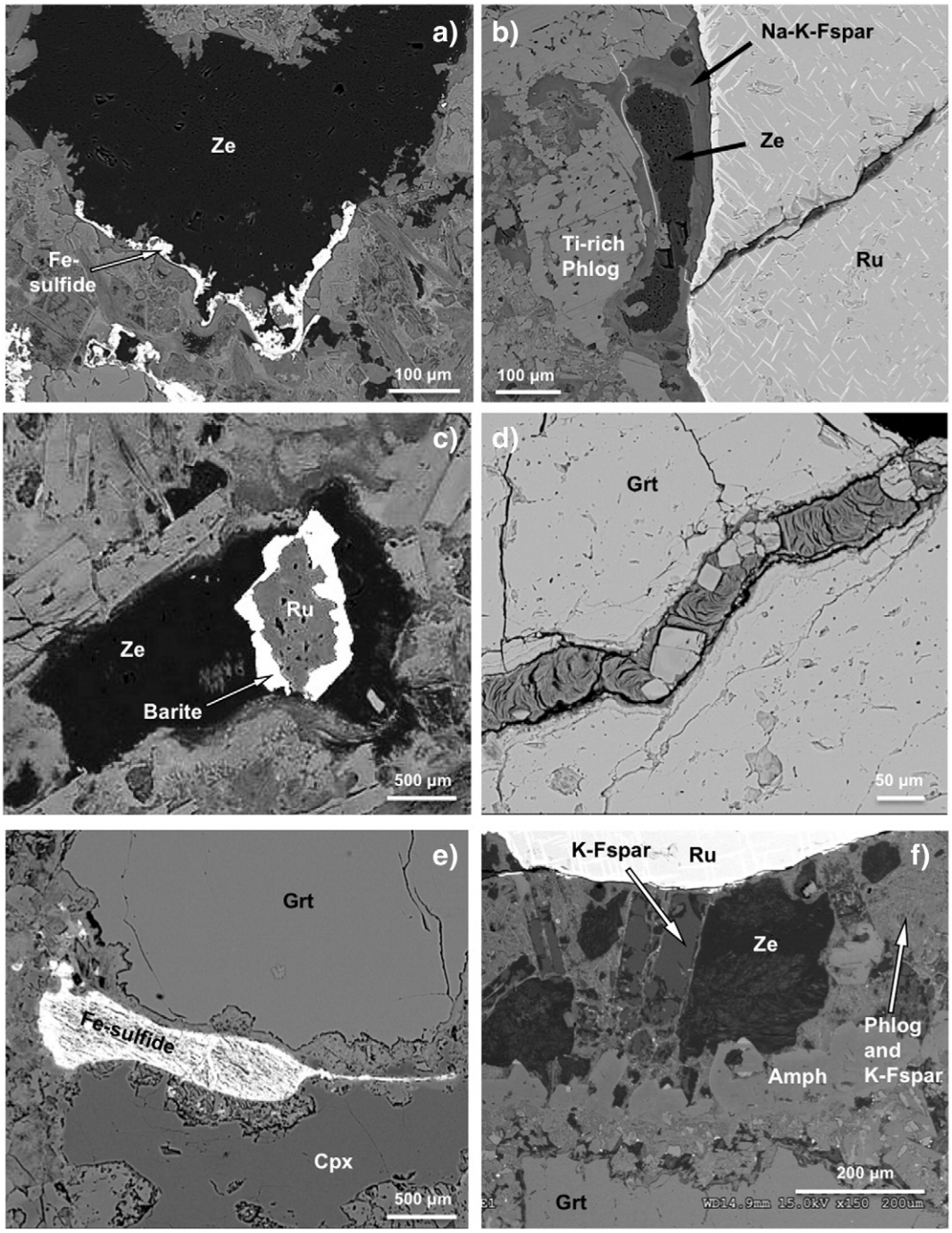

Fig. 4. Back-scattered images of mineral assemblage. (a) Zeolite rimmed by a Fe-sulfide. (b) Secondary mineral assemblage around rutile that contains needles of ilmenite. (c) Rutile rimmed by barite in the melt pool. (d) Calcite crystals in a "veinlet" of silicate gel-like material. In some areas a narrow band of phlogopite is present along the garnet-veinlet contact. (e) Fe-sulfide within the secondary assemblage between garnet and clinopyroxene. (f) Secondary mineral assemblage around rutile, consisting of zeolite, amphibole, needles of K-feldspar and phlogopite and small crystals of spinel. Amph - amphibole, Cpx - clinopyroxene, Grt - garnet, Fspar - feldspar, Phlog - phlogopite, Ru - rutile, Ze - zeolite.

omphacitic clinopyroxene, which has much higher concentrations of Na and Al, and lower amounts of Ca (Table 1).

Sulfide, present both within the secondary mineral assemblage and as inclusions in primary phases, is usually of pure FeS composition with small amounts of Ni and/or Cu. Barite has elevated Sr contents (up to 6 wt% SrO).

Compositional zoning is a common feature for the minerals present within the secondary assemblage. Although almost every single mineral is zoned to a certain extent, the most commonly observed are zoned calcite, which usually has elevated Sr-contents (up to 1.1 wt% SrO) on the rims and phlogopite (with variable Na (0.2–1.6 wt% Na_2O) and Ba (up to 1.5 wt% BaO) contents. Compositional variations in calcite crystals are evident in the back-scattered electron images in Fig. 3d. In Table 1 average compositions of grains are reported.

3.3. Trace element compositions of primary and secondary phases

Normalised trace element diagrams for garnet and primary clinopyroxene are very similar to those reported by Huang et al. (2012) (Fig. 6) for other Type I eclogite xenoliths from the Roberts Victor pipe. The trace element compositions of spongy clinopyroxene with the included small alkali-rich pockets (recrystallised into feldspars)

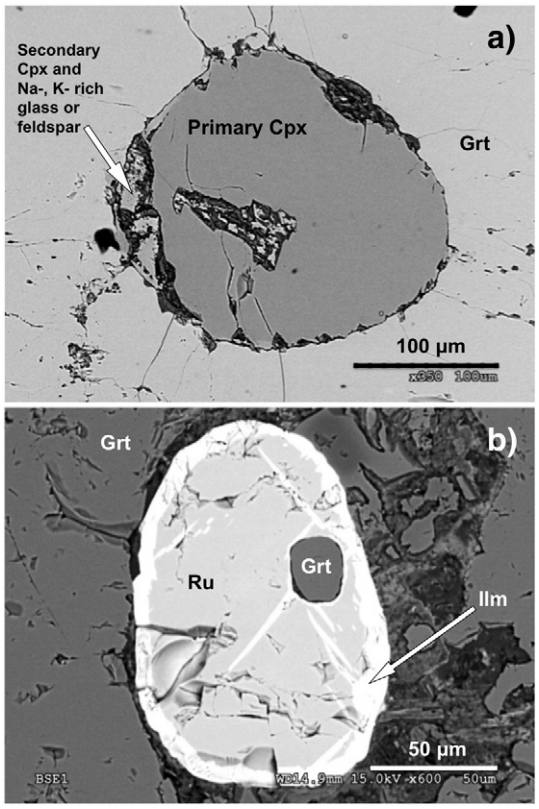

Fig. 5. Back-scattered images of mineral assemblage. (a) Primary clinopyroxene inclusion in garnet showing the melting assemblage at the contact of the two minerals. (b) Garnet inclusion in rutile, showing a thin rim of melting assemblage on the boundary. Ilm - ilmenite.

(Fig. 1b) and the bulk secondary assemblage, represented by multiple quenched phases are presented in Table 2 and Fig. 7.

Despite the presence of interstitial glass-like material (recrystallised into K- and Na-feldspar), ablation of which could not be avoided by 50 μm size laser spot, the spongy clinopyroxene shows an almost identical pattern to the primary clinopyroxene. The main differences are in the elevated LILE (Rb, Ba), LREE (La, Ce) and Th in the spongy clinopyroxene.

On the normalised trace element diagrams (Fig. 7) the secondary mineralisation exhibits features, which may reflect mixtures of components derived from partial melting of both garnet and clinopyroxene. The LREE and LILE parts of the pattern for the secondary minerals are reminiscent of those of the clinopyroxene. Similarly, the HREE (heavy REE) part of the pattern for the secondary minerals may derive from garnet. Ba is significantly elevated over Rb (following the secondary spongy clinopyroxene pattern).

4. Discussion. Melting in the sub-cratonic mantle

4.1. "Spongy" textures in mantle xenoliths

Spongy or sieve-like clinopyroxene and associated alkali-rich glass are very common in ultramafic xenoliths from different tectonic settings (e.g. Carpenter et al., 2002; Ma et al., 2015; Shaw et al., 2006; Su et al., 2011). Melt pockets with usual, partially recrystallised glassy material have also been reported in peridotite xenoliths from many localities (e.g. Schiano and Clocchiatti, 1994; Schiano et al., 1994; Yaxley and Kamenetsky, 1999; Yaxley et al., 1997).

Melt pockets in peridotite samples usually contain secondary pyroxenes, olivine, spinel and a substantial volume of vugs attributed to the presence of a fluid phase (e.g. Ionov et al., 1994; Yaxley and Kamenetsky, 1999). Feldspar and amphibole are less abundant, while calcite is rare (e.g. Su et al., 2010; Yaxley and Kamenetsky, 1999; Yaxley et al., 1997).

Spongy clinopyroxene usually occurs in rims of primary clinopyroxene and the width of the rims can vary greatly from a few microns to hundreds of microns (Su et al., 2011). In some cases, primary clinopyroxene is completely converted into the secondary spongy clinopyroxene (Shaw et al., 2006). The regions of spongy clinopyroxene observed in peridotite xenoliths contain inclusions of spinel, olivine and small pools of alkali-rich glass that vary in composition from nepheline- to quartz-normative (Yaxley and Kamenetsky, 1999).

The origin of melt pockets and spongy textures in secondary clinopyroxene is still a matter of considerable debate. The main hypotheses invoke:

- low-degree partial melting of lithospheric mantle (Draper and Green, 1997; Shaw, 2009)
- percolation of metasomatic fluids/melts of different origins (Carpenter et al., 2002; Ionov et al., 1994; Schiano and Clocchiatti, 1994; Schiano et al., 1994)
- reaction of the xenolith with a host magma (Shaw and Dingwell, 2008)
- breakdown of metasomatic minerals that were formed during previous melting and crystallisation events (Yaxley and Kamenetsky, 1999; Yaxley et al., 1997)
- decompression-induced incongruent melting prior to xenolith entrainment in the host magmas (Su et al., 2011)
- decompression-induced incongruent melting after the entrainment by the host magmas (Misra et al., 2004).

Even though there is no agreement on the exact mechanism of the formation of the spongy clinopyroxene (and other reaction phases), it is obvious that these textures are common in both peridotitic and eclogitic xenoliths and that the presence of melt and its interaction with the primary phases are necessary precursors for their formation.

The composition of the glass-like material associated with the spongy clinopyroxene can be indicative of the primary phases composition. For instance, glass from peridotitic affinities is usually more Mg-rich and with a higher Na_2O/K_2O ratio than the eclogitic (e.g. Ionov et al., 1994; Yaxley and Kamenetsky, 1999). In SS2 xenolith, glass is recrystallised mainly into the K-feldspar, which contains 14.42 wt% K_2O and only 1.14 wt% Na_2O. Potassium-rich glass was also reported by Misra et al. (2004) associated with the spongy clinopyroxene in the Udachnaya pipe eclogites (up to 6.32 wt% K_2O and up to 0.86 wt% Na_2O) and by Liu et al. (2009) for the world's largest diamondiferous eclogite xenolith (UD-111/02), from the Udachnaya kimberlite.

The higher K/Na ratio for the eclogitic secondary mineral assemblage could be characteristic of the primary phlogopite or any other K-bearing phases now absent due to their complete melting. The former presence of primary phlogopite is also consistent with the elevated Ba-contents of the secondary mineral assemblage. However, as discussed below, the presence of primary phlogopite is not necessary, because the abundance of potassium in the bulk secondary assemblage is 0.35 ± 0.31 wt% K_2O. Even if the highest value of ~0.7 wt% K_2O is assumed, fairly low degrees of partial melting of the primary mineral assemblage alone could well account for it.

4.2. Textural evidence for incipient melting

The nature of sub-cratonic mantle metasomatism, as well as the origin of the kimberlite magmas, remain debatable (e.g. Le Roex et al., 2003; Ringwood et al., 1992; Tappe et al., 2013; Tappe et al., 2017). A large number of studies of eclogite xenoliths entrapped in kimberlite reveal significant modification of the primary mineral assemblage and the appearance of a large number of new phases (e.g. Aulbach et al., 2007; Fung and Haggerty, 1995; Huang et al., 2014; Pyle and Haggerty,

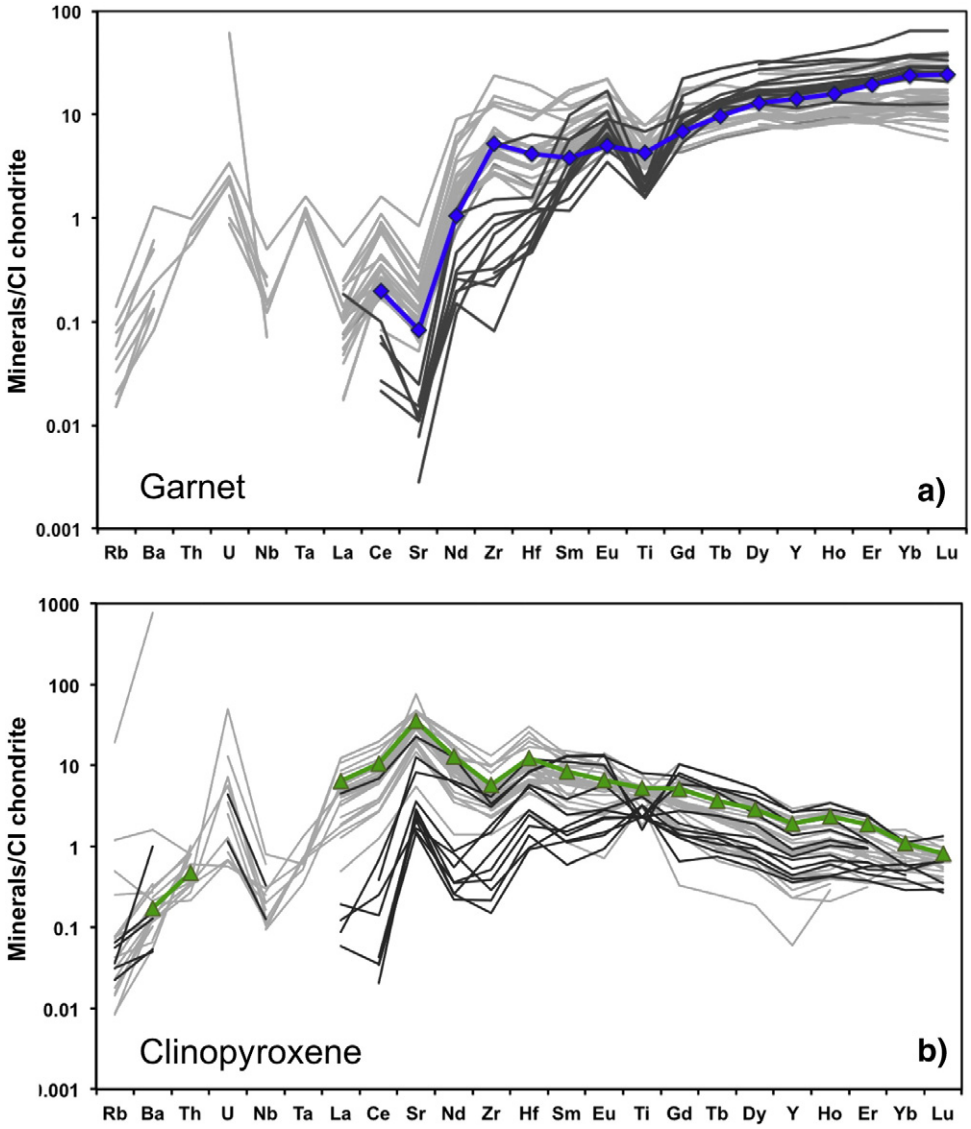

Fig. 6. Trace element patterns of garnet and primary clinopyroxene in comparison with the garnet and clinopyroxene reported by Huang et al. (2012) from Type I (light grey) and Type II (dark grey) Roberts Victor eclogites. All patterns are normalised to CI chondrites (McDonough and Sun, 1995).

1998; Sobolev et al., 1999; Spetsius and Taylor, 2002). Given the high concentrations of incompatible elements (both LILE and high-field-strength elements) found in these secondary minerals, the traditional approach is to attribute crystallisation of the secondary mineral assemblage to modal and cryptic metasomatism prior to the kimberlite magma percolation, to in-situ partial melting due to infiltration of metasomatic fluids and/or to interaction with the kimberlitic magma itself (e.g. Misra et al., 2004; Spetsius and Taylor, 2002). All of these scenarios are plausible; however, none of them explain the nature and origin of the metasomatic fluids, which are evidently abundant in K, Na, Cl, Ca, Ti, Ba, CO_2, H_2O, LREE and other highly incompatible components. Moreover, formation of kimberlitic magmas requires large amounts of these components to be present in the mantle source.

The textures and both primary and secondary mineral assemblages observed in the SS2 xenolith are similar to those reported previously in metasomatically altered eclogite xenoliths (Huang et al., 2014; Misra et al., 2004; Pyle and Haggerty, 1994; Pyle and Haggerty, 1998; Sobolev et al., 1999; Spetsius and Taylor, 2002). On the other hand, we interpret the textural and mineralogical features of this sample as strong evidence for incipient melting of the eclogite. The melting assemblage surrounds absolutely every grain within the primary assemblage. Even in such cases, when one primary mineral is present as a small inclusion in another primary mineral, a small rim with melting products around the inclusion is observed (Fig. 5).

In addition to the silicate-rich melt, it is likely that there existed an immiscible sulfur-rich liquid (Fig. 4a,e). Depending on the P-T-fO_2 conditions and the composition of the silicate, sulfur reaches saturation in silicate melts at ~1000–2000 ppm (e.g. Fortin et al., 2015; Li and Ripley, 2009; Smythe et al., 2016). Even the higher end of this range does not seem to be enough to incorporate all sulfur in the silicate melt. Since at mantle P-T conditions sulfides are usually present in a liquid form (Zhang and Hirschmann, 2016), sulfur segregates into separate, immiscible sulfide liquid, making sulfides quite common in eclogite xenoliths, although still present in fairly low abundances (<2 vol%) (Gréau et al., 2013; Howarth et al., 2015). Under highly oxidised conditions, possibly even sulfate liquids are formed (Giuliani et al., 2013).

4.3. Compositional evidence for the incipient melting

The second type of evidence for incipient melting is compositional. The secondary mineral assemblages that develop on the grain boundaries, along the veins that cut across the xenoliths and in the melt pockets within the garnet crystals, all consist of the same minerals,

Table 2
Trace element compositions of the primary phases and melting assemblage.

	Garnet	σ (17)	Cpx	σ (14)	Cpx spongy+melt	σ (13)	Secondary assemblage	σ (37)
Rb	b.d.l.	–	b.d.l.	–	7.47	1.43	39.9	15.2
Ba	b.d.l.	–	0.42	0.03	83.7	11.5	1161	1090
La	b.d.l.	–	1.53	0.13	3.69	0.99	9.91	3.65
Ce	0.12	0.02	6.42	0.35	10.4	1.98	21.0	10.2
Nd	0.48	0.04	5.87	0.16	7.96	1.02	12.0	7.20
Sr	0.61	0.05	254	2	193	10	277	123
Sm	0.56	0.07	1.24	0.05	1.37	0.07	1.41	0.93
Eu	0.28	0.04	0.37	0.03	0.41	0.03	0.44	0.22
Gd	1.38	0.16	1.02	0.04	1.12	0.11	1.39	0.63
Tb	0.35	0.04	0.13	0.01	0.15	0.01	0.26	0.09
Dy	3.17	0.28	0.71	0.04	0.78	0.06	1.96	0.64
Ho	0.86	0.05	0.13	0.01	0.13	0.01	0.52	0.18
Er	3.12	0.17	0.30	0.03	0.33	0.04	1.79	0.61
Yb	3.83	0.21	0.18	0.03	0.20	0.02	2.12	0.71
Y	22.2	1.19	3.03	0.09	3.30	0.17	13.49	4.37
Lu	0.60	0.06	0.02	0.01	0.020	0.006	0.35	0.11
Ti	1873	154	2294	206	2195	62	4688	3587
Zr	20.1	5.13	21.8	0.55	25.1	1.80	51.5	23.1
Hf	0.43	0.14	1.26	0.10	1.29	0.06	1.56	0.99
Nb	b.d.l.	–	b.d.l.	–	1.58	0.70	15.7	11.9
Ta	b.d.l.	–	b.d.l.	–	0.07	0.03	1.22	0.91
Th	b.d.l.	–	0.014	0.014	0.20	0.04	1.13	0.28
U	b.d.l.	–	b.d.l.	–	0.08	0.04	0.42	0.40

b.d.l. below detection limit.

which are almost identical in composition. If there were a fluid percolating into the eclogite, it would pass along the veins and fractures, and the crystallised secondary phases would be different to the sites of modification unaffected by the fluid.

Similarly to the spongy clinopyroxene, Ba-rich minerals were found in mantle xenoliths in both peridotitic and eclogitic affinities from different localities worldwide (Almeida et al., 2014; Kogarko et al., 2007; Kogarko et al., 2012; Mitchell and Lewis, 1983; Mogarovskii et al., 2007; Pyle and Haggerty, 1998). These include multiple findings of barite (e.g. Pyle and Haggerty, 1998), Ba-rich Ti-phlogopite (Kogarko et al., 2012; Mogarovskii et al., 2007; Kamenetsky et al., 2014), Ba-rich apatite (Kamenetsky et al., 2014) and a number of rare and unusual minerals, like priderite (Almeida et al., 2014), henrymeyerite (Kogarko et al., 2007) and Ba-rich titanates (Almeida et al., 2014). Priderite is a mineral with a formula close to $A_{1.5}M_8O_{16}$ where the A-site is occupied mainly by Ba and K, and M-site by Ti, Fe and Cr, while henrymeyerite is a mineral from the priderite group. These minerals occur within the secondary mineral assemblage, rimming younger generations of rutile or ilmenite (Ba-rich titanites), or, as barite, forming cross cutting veins.

Most authors attribute this barium enrichment to be a result of alkali-rich or carbonate-rich mantle metasomatism (Foley et al., 1994; Kogarko et al., 2012) with high-Ba phlogopite suggested to crystallise at the early stages of magmatic crystallisation (Kogarko et al., 2012). Foley et al. (1994) have synthesised priderite experimentally and have confirmed its stability up to diamond-forming pressures of 5 GPa, supporting the finding of this mineral in diamond inclusions (Jaques et al., 1989).

An alternative explanation for the Ba-enrichment may come from the nature of the eclogitic xenoliths. The observed enrichment in K, Ba and other incompatible elements is inherited and reflects the initial composition of the oceanic crust that has been converted into eclogite. Due to hydrothermal alteration, the upper part of the oceanic crust contains up to a few wt.% of volatiles and significant amounts of P (up to 0.17 wt% P_2O_5), Na (up to 3.30 wt% Na_2O and K (up to 7.3 wt% K_2O) and other incompatible elements (Alt and Teagle, 2003). Ba-enrichment (up to 143 ppm in altered tholeiitic basalts; Alt and Teagle, 2003) derives from the seawater component. The original composition of the altered oceanic crust in terms of minor components is highly uncertain; and their concentrations can vary over an order of magnitude, which probably causes variation in the melting products within the kimberlite xenoliths worldwide. Most of the highly incompatible elements, like LILE, are located in minute phases along grain boundaries. This has been revealed by comparing the bulk-rock compositions to the compositions of the constituent minerals (e.g. Condie et al., 2004; Suzuki, 1987; Yamamoto et al., 2009).

But even if potassium is present only at typical MORB-concentrations, this would be enough to cause the pattern of so-called K-rich metasomatism. According to experimental data, at 3.5–5 GPa potassium is almost completely incompatible and even 0.5 wt% H_2O and 0.4 wt% K_2O in the starting composition at low degrees of melting (~4–7%) produced hydrous, felsic melt with up to 10 wt% K_2O (Kiseeva et al., 2012). Thomson et al. (2016) reported 2.8 wt% Na_2O and 0.29 wt% K_2O at 3 GPa for low degrees melt (~10%) of a carbonated eclogite that contains 2.48 wt% Na_2O and 0.06 wt% K_2O in the starting mixture. To our knowledge, there are no measurements of Ba in experimental melts produced by melting of altered oceanic crust at high pressures, however, given its highly incompatible character, lower degree (<10%) melts will be strongly enriched in Ba.

The fate of incompatible elements (including K, Ba, LREE) and carbon during subduction is still a matter of debate. In their review, Dasgupta and Hirschmann (2010) estimated about half of the subducted carbon is transported into the mantle beyond the sub-arc region. Kelemen and Manning (2015) and Poli (2015) argue that the presence of water (which is ubiquitous in subducted slabs) is drastically depressing the carbonate solidus fluxing CO_2-rich aqueous fluids into the wedge and decreasing the amount of subducted carbonate. Regardless of the amount of carbonate that is currently subducted, there is enough evidence for the presence of recycled crustal components in the upper mantle and even the mantle transition zone (e.g. Stachel and Harris, 2009; Tappert et al., 2005). The amount of calcium within the bulk secondary assemblage is fairly low (~2 wt% CaO), which implies that the carbonate was probably lost during post-magmatic processes.

The Na/K ratio of the glass is partly a function of pressure. As mentioned above, potassium is incompatible at low pressures and becomes compatible only with the stability of K-hollandite at pressures ≥15 GPa (Grassi and Schmidt, 2011; Kiseeva et al., 2013; Wang and Takahashi, 2000). Since Na becomes compatible in the clinopyroxene from about 2.5–3 GPa, lower pressure melts would be both K- and Na-rich. Incipient melting of primary clinopyroxene at pressures <2.5 GPa would result in the formation of more diopsidic secondary clinopyroxene and alkali-rich melt.

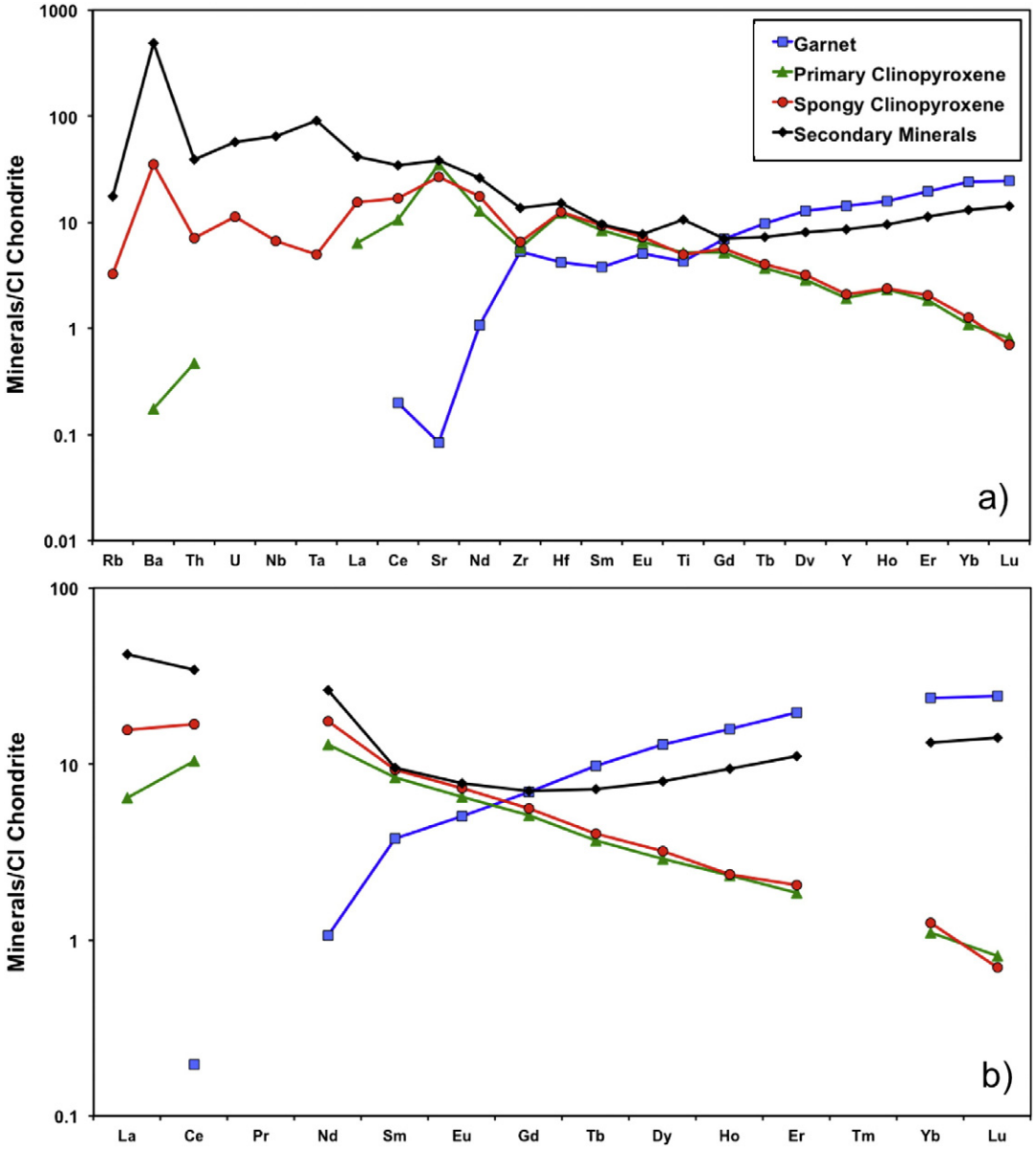

Fig. 7. Trace element patterns of garnet, primary clinopyroxene, secondary clinopyroxene and secondary mineral assemblage normalised to CI chondrites (McDonough and Sun, 1995).

This is commensurate with the secondary mineral assemblage found within primary clinopyroxene grains, which consists of Al- and Na- depleted secondary clinopyroxene and alkali-rich melt pools. Additionally, the alkali-rich nature of the melt together with carbonate-rich components could produce carbonate-silicate immiscible liquids (Kiseeva et al., 2012), resulting in melts pools that are enriched in Na and K.

Thus, the melting assemblage we observe now did not necessarily require any introduction of additional components. In-situ melting alone could produce highly incompatible element enriched melt without the need for involvement of a hypothetical "metasomatic event". Neither compositional nor textural characteristics of the studied xenolith are indicative of whether the melting occurred prior or after the xenolith's entrainment by the host kimberlite magma. The trigger mechanism for the incipient melting is likely to be either decompression and/or heating. Su et al. (2011) arrived at a similar conclusion, however the authors argued that only the major element pattern may be explained by the incipient melting.

Importantly, in order to produce a metasomatic melt or fluid in the mantle, a mantle lithology is required to partially melt, and there are only two possible sources that could produce melts in the cratonic mantle – peridotites and eclogites. Once these mantle-derived fluids segregate from their source, they may be out of equilibrium with the wallrock through which they migrate, acting as a flux, reacting with the wall rock, triggering its partial melting and causing so-called "mantle metasomatism".

5. Conclusions

By using petrological, compositional and experimental evidence, we conclude that the altered oceanic crust represented by an eclogite in the deep mantle is a plausible source of mantle metasomatic fluids and melts. Changes in P-T conditions can cause initiation of melting, and in this case there is no requirement for an external "influence" on the observed "melting assemblage".

On the other hand, it is still possible that there could be some influence from the external fluids. The proportion of externally and internally derived fluids could be variable and it is impossible to discern between the two of them. However, any externally derived fluid would need a source rock that is likely to be an eclogite and that is taking us back to the "chicken or egg dilemma".

Acknowledgements

We thank Larry Taylor, Geoffrey Howarth and an anonymous reviewer for thorough and constructive reviews. We are also grateful to Sebastian Tappe and Klaus Mezger for editorial comments and handling. The research in Oxford University was financially supported by NERC grant NE/L010828/1 to ESK and by European Research Council grant 267764 to B. Wood. Research at ANU was supported by ARC Future Fellowship to GMY.

References

Almeida, V.V., Janasi, V.D.A., Svisero, D.P., Nannini, F., 2014. Mathiasite-loveringite and priderite in mantle xenoliths from the Alto Paranaíba Igneous Province, Brazil: genesis and constraints on mantle metasomatism. Central European Journal of Geosciences 6 (4), 614–632.

Alt, J.C., Teagle, D.A.H., 2003. Hydrothermal alteration of upper oceanic crust formed at a fast-spreading ridge: mineral, chemical, and isotopic evidence from ODP Site 801. Chem. Geol. 201 (3–4), 191–211.

Aulbach, S., Pearson, N.J., O'Reilly, S.Y., Doyle, B.J., 2007. Origins of xenolithic eclogites and pyroxenites from the central Slave craton, Canada. J. Petrol. 48 (10), 1843–1873.

Carpenter, R.L., Edgar, A.D., Thibault, Y., 2002. Origin of spongy textures in clinopyroxene and spinel from mantle xenoliths, Hessian Depression, Germany. Mineral. Petrol. 74 (2–4), 149–162.

Condie, K.C., Cox, J., O'Reilly, S.Y., Griffin, W.L., Kerrich, R., 2004. Distribution of high field strength and rare earth elements in mantle and lower crustal xenoliths from the southwestern United States: the role of grain-boundary phases. Geochim. Cosmochim. Acta 68 (19), 3919–3942.

Dasgupta, R., Hirschmann, M.M., 2010. The deep carbon cycle and melting in Earth's interior. Earth Planet. Sci. Lett. 298 (1–2), 1–13.

Dawson, J.B., 1984. In: Kornprobst, J. (Ed.), Contrasting types of upper-mantle metasomatism? In Kimberlites II: The mantle and crust-mantle relationships. Elsevier, pp. 289–294.

Draper, D.S., Green, T.H., 1997. P-T phase relations of silicic, alkaline, aluminous mantle-xenolith glasses under anhydrous and C-O-H fluid-saturated conditions. J. Petrol. 38 (9), 1187–1224.

Ellis, D.J., Green, D.H., 1979. Experimental study of the effect of Ca upon garnet-clinopyroxene Fe-Mg exchange equilibria. Contrib. Mineral. Petrol. 71 (1), 13–22.

Foley, S., Hofer, H., Brey, G., 1994. High-pressure synthesis of priderite and members of the lindsleyite-mathiasite and hawthorneite-yimengite series. Contrib. Mineral. Petrol. 117 (2), 164–174.

Fortin, M.-A., Riddle, J., Desjardins-Langlais, Y., Baker, D.R., 2015. The effect of water on the sulfur concentration at sulfide saturation (SCSS) in natural melts. Geochim. Cosmochim. Acta 160, 100–116.

Fung, A.T., Haggerty, S.E., 1995. Petrography and mineral compositions of eclogites from the Koidu kimberlite complex, Sierra-Leone. Journal of Geophysical Research-Solid Earth 100 (B10), 20451–20473.

Giuliani, A., et al., 2013. Mantle oddities: a sulphate fluid preserved in a MARID xenolith from the Bultfontein kimberlite (Kimberley, South Africa). Earth Planet. Sci. Lett. 376, 74–86.

Goldschmidt, V.M., 1922. On the metasomatic processes in silicate rocks. Econ. Geol. 17, 105–123.

Grassi, D., Schmidt, M., 2011. Melting of carbonated pelites at 8–13 GPa: generating K-rich carbonatites for mantle metasomatism. Contrib. Mineral. Petrol. 162 (1), 169–191.

Gréau, Y., et al., 2011. Type I eclogites from Roberts Victor kimberlites: products of extensive mantle metasomatism. Geochim. Cosmochim. Acta 75 (22), 6927–6954.

Gréau, Y., Alard, O., Griffin, W.L., Huang, J.X., O'Reilly, S.Y., 2013. Sulfides and chalcophile elements in Roberts Victor eclogites: unravelling a sulfide-rich metasomatic event. Chem. Geol. 354, 73–92.

Heaman, L.M., Creaser, R.A., Cookenboo, H.O., Chacko, T., 2006. Multi-stage modification of the northern Slave mantle lithosphere: evidence from zircon- and diamond-bearing eclogite xenoliths entrained in Jericho kimberlite, Canada. J. Petrol. 47 (4), 821–858.

Howarth, G.H., et al., 2015. 3-D X-ray tomography of diamondiferous mantle eclogite xenoliths, Siberia: a review. J. Asian Earth Sci. 101, 39–67.

Huang, J.X., Gréau, Y., Griffin, W.L., O'Reilly, S.Y., Pearson, N.J., 2012. Multi-stage origin of Roberts Victor eclogites: progressive metasomatism and its isotopic effects. Lithos 142, 161–181.

Huang, J.-X., et al., 2014. Unmasking xenolithic eclogites: progressive metasomatism of a key Roberts Victor sample. Chem. Geol. 364, 56–65.

Ionov, D.A., Hofmann, A.W., Shimizu, N., 1994. Metasomatism-induced melting in mantle xenoliths from Mongolia. J. Petrol. 35 (3), 753–785.

Jaques, A.L., et al., 1989. Composition of crystalline inclusions and C-isotopic composition of Argyle and Ellendale diamonds. In: Jaques, A.L., Ferguson, J., D.H., G. (Eds.), Kimberlites and related rocks 2: their crust/mantle setting, diamonds, and diamond exploration. Blackwells, Melbourne, pp. 966–989.

Kamenetsky, V.S., et al., 2014. Chemical abrasion of zircon and ilmenite megacrysts in the Monastery kimberlite: Implications for the composition of kimberlite melts. Chem. Geol. 383, 76–85.

Kelemen, P.B., Manning, C.E., 2015. Reevaluating carbon fluxes in subduction zones, what goes down, mostly comes up. Proc. Natl. Acad. Sci.

Kiseeva, E.S., et al., 2012. An experimental study of carbonated eclogite at 3·5–5·5 GPa – implications for silicate and carbonate metasomatism in the cratonic mantle. J. Petrol. 53 (4), 727–759.

Kiseeva, E.S., Litasov, K.D., Yaxley, G.M., Ohtani, E., Kamenetsky, V.S., 2013. Melting and phase relations of carbonated eclogite at 9–21 GPa and the petrogenesis of alkali-rich melts in the deep mantle. J. Petrol. 54 (8), 1555–1583.

Kogarko, L.N., Kurat, G., Ntaflos, T., 2007. Henrymeyerite in the metasomatized upper mantle of eastern Antarctica. Can. Mineral. 45, 497–501.

Kogarko, L.N., Ryabchikov, I.D., Kuzmin, D.V., 2012. High-Ba mica in olivinites of the Guli massif (Maimecha–Kotui province, Siberia). Russ. Geol. Geophys. 53 (11), 1209–1215.

Krogh, E.J., 1988. The garnet-clinopyroxene Fe-Mg geothermometer - a reinterpretation of existing experimental data. Contrib. Mineral. Petrol. 99 (1), 44–48.

Le Roex, A.P., Bell, D.R., Davis, P., 2003. Petrogenesis of group I kimberlites from Kimberley, South Africa: evidence from bulk-rock geochemistry. J. Petrol. 44 (12), 2261–2286.

Li, C.S., Ripley, E.M., 2009. Sulfur contents at sulfide-liquid or anhydrite saturation in silicate melts: empirical equations and example applications. Econ. Geol. 104 (3), 405–412.

Liu, Y., et al., 2009. Metasomatic origin of diamonds in the world's largest diamondiferous eclogite. Lithos 112 (Supplement 2), 1014–1024.

Ma, G.S.-K., et al., 2015. Melt pockets and spongy clinopyroxenes in mantle xenoliths from the Plio-Quaternary Al Ghab volcanic field, NW Syria: implications for the metasomatic evolution of the lithosphere. In: Khan, A., Deschamps, F. (Eds.), The Earth's Heterogeneous Mantle: A Geophysical, Geodynamical, and Geochemical Perspective. Springer International Publishing, Cham, pp. 205–257.

MacGregor, I.D., Carter, J.L., 1970. The chemistry of clinopyroxenes and garnets of eclogite and peridotite xenoliths from the Roberts Victor mine, South Africa. Phys. Earth Planet. Inter. 3, 391–397.

McCandless, T.E., Gurney, J.J., 1989. Sodium in garnet and potassium in clinopyroxene: criteria for classifying mantle eclogites. In: Ross, J., Jaques, A.L., Ferguson, J., Green, D.H., O'Reilly, S.Y., Danchin, R.V., Janse, A.J.A. (Eds.), Kimberlites and Related Rocks. Geological Society of Australia, Special Publication, Perth, pp. 827–832.

McDonough, W.F., Sun, S.S., 1995. The composition of the Earth. Chem. Geol. 120 (3–4), 223–253.

Misra, K.C., Anand, M., Taylor, L.A., Sobolev, N.V., 2004. Multi-stage metasomatism of diamondiferous eclogite xenoliths from the Udachnaya kimberlite pipe, Yakutia, Siberia. Contrib. Mineral. Petrol. 146 (6), 696–714.

Mitchell, R.H., Lewis, R.D., 1983. Priderite-bearing xenoliths from the Prairie Creek mica peridotite, Arkansas. Can. Mineral. 21 (Feb), 59–64.

Mogarovskii, V.V., Lutkov, V.S., Lutkova, V.Y., 2007. Barium and strontium in the upper mantle of the Pamirs and Tien Shan. Geochem. Int. 45 (7), 685–697.

Poli, S., 2015. Carbon mobilized at shallow depths in subduction zones by carbonatitic liquids. Nat. Geosci. advance online publication.

Pyle, J.M., Haggerty, S.E., 1994. Silicate-carbonate liquid immiscibility in upper-mantle eclogites - implications for natrosilicic and carbonatitic conjugate melts. Geochim. Cosmochim. Acta 58 (14), 2997–3011.

Pyle, J.M., Haggerty, S.E., 1998. Eclogites and the metasomatism of eclogites from the Jagersfontein Kimberlite: punctuated transport and implications for alkali magmatism. Geochim. Cosmochim. Acta 62 (7), 1207–1231.

Ringwood, A.E., Kesson, S.E., Hibberson, W., Ware, N., 1992. Origin of kimberlites and related magmas. Earth Planet. Sci. Lett. 113 (4), 521–538.

Schiano, P., Clocchiatti, R., 1994. Worldwide occurrence of silica-rich melts in sub-continental and sub-oceanic mantle minerals. Nature 368 (6472), 621–624.

Schiano, P., Clocchiatti, R., Shimizu, N., Weis, D., Mattielli, N., 1994. Cogenetic silica-rich and carbonate-rich melts trapped in mantle minerals in Kerguelen ultramafic xenoliths: implications for metasomatism in the oceanic upper mantle. Earth Planet. Sci. Lett. 123 (1–4), 167–178.

Schulze, D.J., Valley, J.W., Spicuzza, M.J., 2000. Coesite eclogites from the Roberts Victor kimberlite, South Africa. Lithos 54 (1–2), 23–32.

Shaw, C.S.J., 2009. Textural development of amphibole during breakdown reactions in a synthetic peridotite. Lithos 110 (1–4), 215–228.

Shaw, C.S.J., Dingwell, D.B., 2008. Experimental peridotite-melt reaction at one atmosphere: a textural and chemical study. Contrib. Mineral. Petrol. 155 (2), 199–214.

Shaw, S.J., Heidelbach, F., Dingwell, D.B., 2006. The origin of reaction textures in mantle peridotite xenoliths from Sal Island, Cape Verde: the case for "metasomatism" by the host lava. Contrib. Mineral. Petrol. 151 (6), 681–697.

Smythe, D.J., Wood, B.J., Kiseeva, E.S., 2016. The S content of silicate melts at sulfide saturation: new experiments and a model incorporating the effects of sulfide composition. Am. Mineral. http://dx.doi.org/10.2138/am-2017-5800CCBY.

Sobolev, V.N., et al., 1999. Quantifying the effects of metasomatism in mantle xenoliths: constraints from secondary chemistry and mineralogy in Udachnaya eclogites, Yakutia. Int. Geol. Rev. 41 (5), 391–416.

Spetsius, Z., Taylor, L., 2002. Partial melting in mantle eclogite xenoliths: connections with diamond paragenesis. Int. Geol. Rev. 44 (11), 973–987.

Stachel, T., Harris, J.W., 2009. Formation of diamond in the Earth's mantle. J. Phys. Condens. Matter 21 (36).

Su, B.X., et al., 2010. Formation of melt pocket in mantle peridotite xenolith from Western Qinling, Central China: partial melting and metasomatism. J. Earth Sci. 21 (5), 641–668.

Su, B.X., et al., 2011. The origin of spongy texture in minerals of mantle xenoliths from the Western Qinling, central China. Contrib. Mineral. Petrol. 161 (3), 465–482.

Suzuki, K., 1987. Grain-boundary enrichment of incompatible elements in some mantle peridotites. Chem. Geol. 63 (334), 319.

Tappe, S., Pearson, D.G., Kjarsgaard, B.A., Nowell, G., Dowall, D., 2013. Mantle transition zone input to kimberlite magmatism near a subduction zone: Origin of anomalous Nd-Hf isotope systematics at Lac de Gras, Canada. Earth Planet. Sci. Lett. 371, 235–251.

Tappe, S., Brand, N.B., Stracke, A., van Acken, D., Liu, C.-Z., Strauss, H., Wu, F.-Y., Luguet, A., Mitchell, R.H., 2017. Plates or plumes in the origin of kimberlites: U/Pb perovskite and Sr-Nd-Hf-Os-C-O isotope constraints from the Superior craton (Canada). Chem. Geol. 455, 52–78 (in this issue).

Tappert, R., et al., 2005. Subducting oceanic crust: the source of deep diamonds. Geology 33 (7), 565–568.

Thomson, A.R., Walter, M.J., Kohn, S.C., Brooker, R.A., 2016. Slab melting as a barrier to deep carbon subduction. Nature 529 (7584), 76–79.

Wang, W.Y., Takahashi, E., 2000. Subsolidus and melting experiments of K-doped peridotite KLB-1 to 27 GPa: its geophysical and geochemical implications. J. Geophys. Res. Solid Earth 105 (B2), 2855–2868.

Yamamoto, J., et al., 2009. Intergranular trace elements in mantle xenoliths from Russian Far East: example for mantle metasomatism by hydrous melt. Island Arc 18 (1), 225–241.

Yaxley, G.M., Kamenetsky, V., 1999. In situ origin for glass in mantle xenoliths from southeastern Australia: insights from trace element compositions of glasses and metasomatic phases. Earth Planet. Sci. Lett. 172 (1–2), 97–109.

Yaxley, G.M., Kamenetsky, V., Green, D.H., Falloon, T.J., 1997. Glasses in mantle xenoliths from western Victoria, Australia, and their relevance to mantle processes. Earth Planet. Sci. Lett. 148 (3–4), 433–446.

Zhang, Z., Hirschmann, M.M., 2016. Experimental constraints on mantle sulfide melting up to 8 GPa. Am. Mineral. 101 (1–2), 181–192.